



**HAL**  
open science

# Structure and Magnetic Properties of Pseudo-1D Chromium Thiolate Coordination Polymers

Andrew Ritchhart, Alexander S. Filatov, Ie-Rang Jeon, John S Anderson

► **To cite this version:**

Andrew Ritchhart, Alexander S. Filatov, Ie-Rang Jeon, John S Anderson. Structure and Magnetic Properties of Pseudo-1D Chromium Thiolate Coordination Polymers. *Inorganic Chemistry*, 2023, 62 (6), pp.2817-2825. 10.1021/acs.inorgchem.2c03991 . hal-04016009

**HAL Id: hal-04016009**

**<https://hal.science/hal-04016009v1>**

Submitted on 17 Apr 2023

**HAL** is a multi-disciplinary open access archive for the deposit and dissemination of scientific research documents, whether they are published or not. The documents may come from teaching and research institutions in France or abroad, or from public or private research centers.

L'archive ouverte pluridisciplinaire **HAL**, est destinée au dépôt et à la diffusion de documents scientifiques de niveau recherche, publiés ou non, émanant des établissements d'enseignement et de recherche français ou étrangers, des laboratoires publics ou privés.



Distributed under a Creative Commons Attribution - NonCommercial 4.0 International License

# The Structure and Magnetic Properties of Pseudo-1D Chromium Thiolate Coordination Polymers

*Andrew Ritchhart,<sup>a</sup> Alexander S. Filatov,<sup>a</sup> Je-Rang Jeon,<sup>b</sup> and John S. Anderson<sup>a†</sup>*

a. Department of Chemistry, University of Chicago, Chicago, Illinois 60637, US

b. Université de Rennes, Institut des Sciences Chimiques de Rennes, UMR CNRS 6226,  
35042 Rennes, France

<sup>†</sup> jsanderson@uchicago.edu

KEYWORDS: Coordination Polymers, Magnetic Polymers, One dimensional

## Abstract

The synthesis, structure, and magnetic properties of two novel, pseudo-1D chromium thiolate coordination polymers (CPs), CrBTT and Cr<sub>2</sub>BDT<sub>3</sub>, are reported. The structures of these materials were determined using X-ray powder diffraction revealing highly symmetric 1D chains embedded within a CP framework. The magnetic coupling of this chain system was measured by SQUID magnetometry, revealing a switch from antiferromagnetic to ferromagnetic behavior dictated by the angular geometrical constraints within the CP scaffold consistent with the Goodenough-Kanamori-Anderson rules. Intrachain magnetic coupling constants  $J_{NN}$  of  $-32.0$  K and  $+5.7$  K were found for CrBTT and Cr<sub>2</sub>BDT<sub>3</sub> respectively using the 1D Bonner-Fisher model of magnetism. The band structure of these materials has also been examined by optical spectroscopy and Density Functional Theory (DFT) calculations revealing semiconducting behavior. Our

findings here demonstrate how CP scaffolds can support idealized low-dimensional structural motifs and dictate magnetic interactions through tuning of geometry and inter-spin couplings.

## Introduction

Low-dimensional material morphologies provide exceptional opportunities for the study and application of physical phenomena. For instance, one and two-dimensional systems often exhibit optical, magnetic, and electronic behaviors that are rare or not possible in three dimensional materials.<sup>1-4</sup> The extremely high planar conductivity of graphene sheets<sup>5</sup> as well as the nonlinear behavior and superconductivity observed in various nanowires<sup>6-8</sup> are examples of such extreme electronic properties arising specifically from low dimensionality. The effect of dimensionality on magnetic order is similarly well-studied, especially in two dimensions.<sup>9,10</sup> In addition to enabling exotic properties, high symmetry in these systems can also present idealized cases with which to study underlying physical phenomena; fewer assumptions are typically required to model physical properties in symmetric 1 and 2D systems than in more complex 3D analogues.

Tunable magnetic phase transitions, spin-centers, and electromagnetic coupling behavior are all desirable properties of functional magnetic materials. Low dimensional magnetic materials are particularly appealing for their potential applications in data storage,<sup>11</sup> quantum computing,<sup>12</sup> ultracold magnetic refrigeration,<sup>13</sup> and sensing.<sup>14</sup> Cr metal organic frameworks in particular have been shown to have strong gas phase selectivity arising from spin interactions with Cr.<sup>15</sup> Additionally more tractable and controllable coupling schemes have made 1 and 2D systems highly desirable magnetic models for several decades.<sup>16-19</sup> Many approaches to design low dimensional magnetic materials have been taken including coordination polymers (CPs) of ions as well as single molecules,<sup>20-24</sup> Van der Waals solids,<sup>25,26</sup> and cluster chemistries.<sup>27-29</sup> However, thus far the majority of these 1D materials are not highly symmetric, often containing skewed zig-

zag motifs,<sup>30,31</sup> multiple magnetic sites<sup>32</sup>, or alternating metal coordination geometries.<sup>25</sup> Moreover many of the most well-studied chains, such as those in the hexagonal perovskite family,<sup>33</sup> are the product of salt melt syntheses which frequently produce electronically limited oxide materials that are not easily tuned. The limited tunability and deviations from ideality in existing systems greatly complicate analyses of underlying magnetic properties; fits to simple magnetic models are often imperfect.<sup>34</sup>

In principle the reticular nature of CP chemistry should be well-suited for systematic adjustments and preservation of symmetry. Here we report a family of Cr thiolate ligand frameworks which enforce highly symmetric 1D chain structures. The CrBTT (**1**, BTT = 1,3,5-benzenetrithiolate) and Cr<sub>2</sub>BDT<sub>3</sub> (**2**, BDT = 1,4-benzenedithiolate) structures represent an unusually high symmetry magnetic chain material (Fig. 2). By taking advantage of the reticular nature of CP chemistry we have synthesized these two structurally related materials where the 1D chain structure is maintained with only slightly modified metal-metal distances and bond angles. These slight intrachain distortions lead to switching between antiferromagnetic (AFM) and ferromagnetic (FM) coupling. Fitting this magnetic behavior with the Bonner-Fisher model of 1D magnetism provides good agreement and allows the determination of the *J* coupling for each compound. Comparison of this coupling with previously reported Cr<sub>2</sub>(SR)<sub>3</sub> motifs reveals competition between direct exchange and superexchange and underscores how geometric tuning supports the unusual FM behavior of **2**. Finally, a series of spectroscopic and computational analyses shows that these materials are semiconducting and further corroborates the magnetic observations. This set of complexes illustrates how rigidly embedding magnetically or electronically interesting motifs within CP frameworks can enable both idealized control over physical properties as well as subtle tuning of intrachain couplings via structural perturbations.

## Results and Discussion:

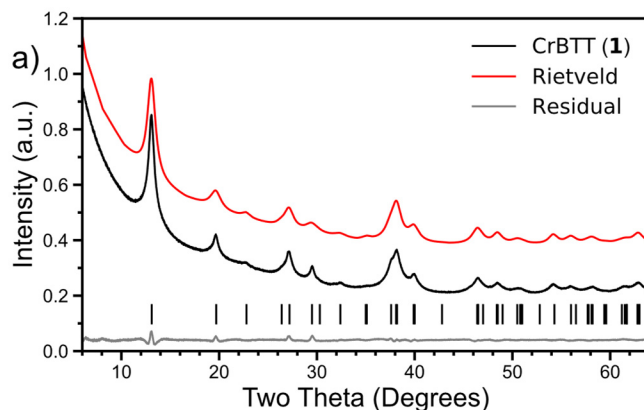
### *Synthesis and Structural Determination*

Solution syntheses of CrBTT (**1**) and Cr<sub>2</sub>BDT<sub>3</sub> (**2**) were performed using rigorously dried solvents under nitrogen atmosphere. A solvothermal synthesis was employed using 1.0 eq of Cr precursor with a slight excess of the thiolate ligands, 1.25 eq of BTT or 2.0 eq of BDT respectively, which resulted in dark red precipitates. For **1**, the highest quality material can be produced by using CrCl<sub>2</sub> in DMF solvent at 120 °C. In contrast, the best synthesis of **2** uses Cr(OTf)<sub>2</sub> in acetonitrile at 75 °C. We note that other combinations of precursors, specifically CrCl<sub>2</sub>, DMF, and BDT, result in additional related but unidentified phases (Fig. S1). The purified Cr thiolate CPs **1** and **2** are air-stable below 100 °C and are stable below 225 °C under inert gas (Fig. S2). Composition analysis with X-ray photoelectron (XPS) spectroscopy, X-ray fluorescence (XRF) spectroscopy, combustion analysis, and Inductively Coupled Plasma – Mass Spectrometry (ICP-MS) all support the assigned formulas of both materials (Figs. S3 and S4 and Tables S5 and S6). While these formulas support formally Cr(III) centers, no product is obtained when Cr(III) starting reagents are used which implies in-situ redox reactivity during the solvothermal synthesis.

X-ray photoelectron spectroscopy (XPS) data were collected on pressed pellet samples of **1** and **2** affixed on conductive carbon tape calibrated relative to the C 1s signal (Fig. S3). Both samples show extremely similar XPS spectra suggesting similar structures and bonding for both materials. The Cr 2p<sup>3/2</sup> peak at 575.6 eV is in exact agreement with the literature assignment of Cr(III) with no apparent multiplet splitting as might be expected for Cr(0), or Cr(II) signals. In the C 1s regions the relative ratio of C–S to C–C/C–H signals integrates accurately to 1:1 and 1:2 for **1** and **2** as expected. The S 2p<sup>3/2</sup> peak at 162.6 eV is consistent with metal-bound thiolates such as well-

studied Au thiolates.<sup>35,36</sup> The S region of **2** shows an additional shoulder visible at 166.0 eV. This position is consistent with an oxidized S which, in addition to the F 1s peak at 688.0 eV, we assign as belonging to residual triflate from the synthesis.<sup>37</sup> We propose that this triflate is charge balancing undercoordinated surface Cr sites, a hypothesis supported by the roughly 1:3.2 Cr:S ratio observed via XRF and ICP analysis (Fig. S4 and Table S6). IR spectroscopy precludes the presence of any free thiols which appear at  $\sim 2560\text{ cm}^{-1}$  (Fig. S7).

Powder diffraction data of **1** and **2** were collected using Cu K $\alpha$  radiation and used to perform crystallographic indexing (Fig. 1). The theoretical structures were modeled programmatically using the indexed cell parameters and symmetry with Cr–S bond lengths of 2.39(2) Å determined from Cr K-edge EXAFS spectra (Fig. S8). Theoretical crystal structure diffraction patterns were generated and refined against the experimental patterns by Rietveld refinement in GSAS-II<sup>38</sup> resulting in residual errors below 2% and 5% for **1** and **2** respectively.



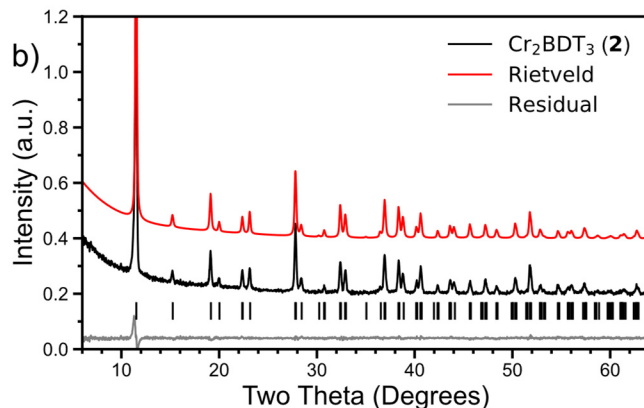


**Figure 1.** Experimental powder X-ray diffractograms (black) and corresponding Rietveld refinement patterns (red) for a) CrBTT (**1**) (CCDC 2203181)  $R_f = 1.1\%$  and b)  $\text{Cr}_2\text{BDT}_3$  (**2**) (CCDC 2203182)  $R_f = 4.9\%$ . Collected with Cu  $K\alpha$ .

The solved structures show chains of face-sharing stacked octahedra within the CP framework with  $P6_3/m$  and  $R-3$  symmetry for **1** and **2** respectively (Fig. 2). These high symmetry space groups provide a great deal of structural information. The Cr–Cr distance is equal to exactly half the length of the trigonal cell c-axis, 3.032(1) Å in **1** and 3.2347(4) Å in **2**. These lengths are slightly longer than the sum of covalent radii<sup>39</sup> for a Cr–Cr bond of 2.78(2) Å but both lie within the range for reported single-bond dichromium molecular complexes.<sup>40–42</sup> In many of these cases, a Cr–Cr bond is typically invoked, but we have not depicted such a bond, for electronic and magnetic reasons discussed below we assign at most a partial bond to only **1**. The combination of high symmetry space groups with completely indexed reflections precludes structural distortions such as bends and inhomogeneous bonds which would increase the unit cell or lower the symmetry.

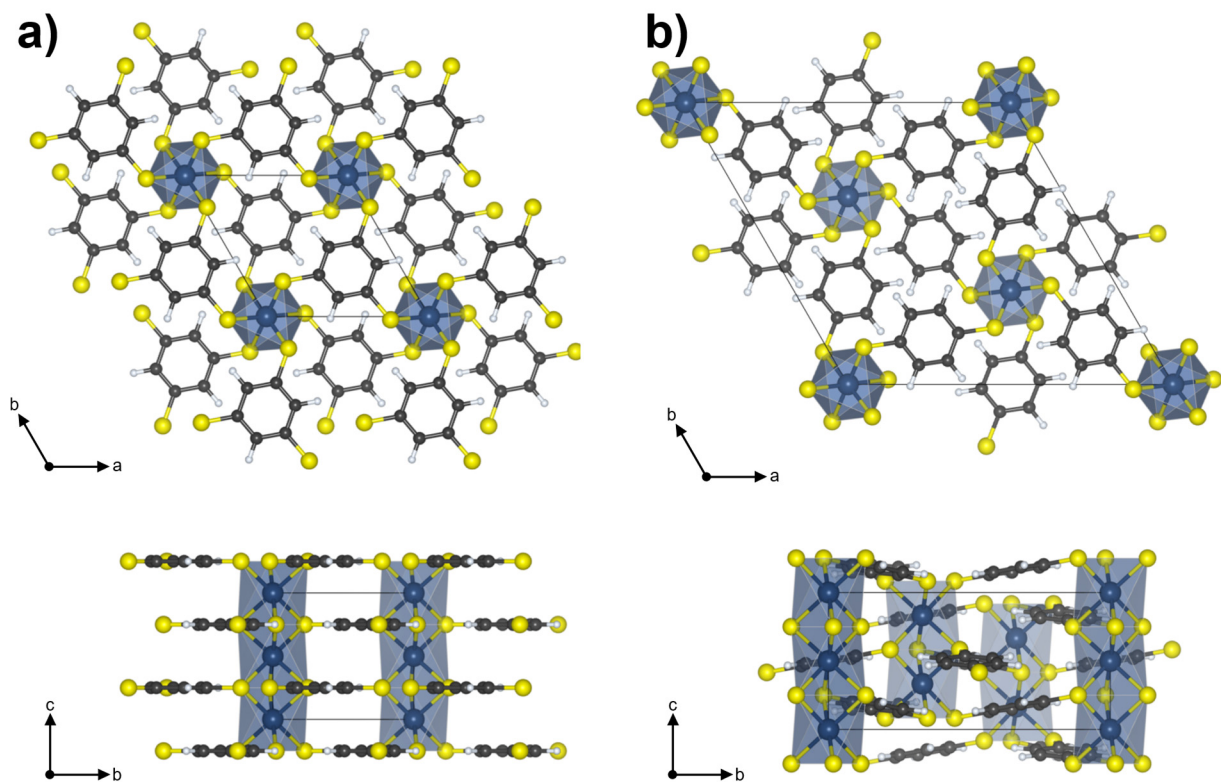


**Figure 2.** The refined CP structure unit cells as viewed along the c and a axes with  $(\text{CrS}_3)_n$  chains depicted as metal-centered polyhedra. (a) The structure of CrBTT (**1**),  $a = 7.821(3) \text{ \AA}$ ,  $c = 6.064(1) \text{ \AA}$ . (b) The structure of Cr<sub>2</sub>BDT<sub>3</sub> (**2**),  $a = 15.382(1) \text{ \AA}$ ,  $c = 6.4693(4) \text{ \AA}$ , depicted here in the trigonal rather than rhombohedral unit cell for comparison.

In both **1** and **2** the octahedral Cr–S environment is elongated along the c-axis. This elongation reduces the symmetry around Cr from  $O_h$  to trigonal antiprismatic ( $D_{3d}$ ) in both cases. This elongation more critically manipulates both the Cr–Cr distance as discussed above and also the Cr–S–Cr bond angle from  $78.0(6)^\circ$  to  $85.2(7)^\circ$  (**1** and **2** respectively). All metal environments are symmetrically identical with no trigonal prismatic centers. In **1** the pseudo-1D chains are interconnected by BTT ligands exactly perpendicular to the primary axis. In contrast, in **2** BDT ligands interconnect the Cr–S chains with an alternating up-down pattern resulting in an A-B-C



ordering of chains in the trigonal unit cell. The ligand and structure differences result in interchain Cr–Cr distances of 7.82 Å and 8.95 Å for **1** and **2** respectively which is long enough to minimize interchain coupling, especially relative to salt-based systems where chains are typically separated by a single alkali metal atom with net interchain distances  $< 6$  Å.<sup>43–45</sup> We observe low bulk conductivity suggesting interchain conjugation is weak despite the aromatic linkers. Also, while there is some empty volume in the frameworks both structures are effectively nonporous and have no detectable BET adsorption by N<sub>2</sub> adsorption analyses (Fig. S9).

Nanowires of stacked metal centers have been observed in the chalcogenides of Hf, Nb, and Ta and some of these cases exhibit novel properties including huge magnetoresistance and superconductivity.<sup>46–49</sup> These freestanding wires are often low in symmetry, with mixed chalcogenide oxidation states and susceptibility to torsion resulting in non-uniform and poorly characterized metal environments in the bulk. Van der Waals solids in the hexagonal perovskite family such as Ba<sub>x</sub>CrS<sub>y</sub>,<sup>44</sup> CoCaO<sub>3</sub>,<sup>25</sup> and others such as CrSbSe<sub>3</sub><sup>26</sup> exhibit analogous stacked structures, however with mixed  $D_{3d}$  and  $D_{3h}$  metal coordination. Inconsistent experimental spin values in these systems are proposed to arise from mixed field splitting which, along with convoluting interchain coupling, often complicates magnetic interpretation. Thus, unbroken octahedral face stacking is a rare feature among stacked 1D CPs and allows us to unambiguously assign spin values and a coupling hierarchy in **1** and **2**. Combined with the mono-metallic composition, and the favorable interchain separation, **1** and **2** represent idealized, analytically tractable magnetic chains with identical symmetry and only minor structural perturbations between them. In total, by changing the ligand from BTT to BDT the spacing between magnetic centers can be modulated from 3.03 Å to 3.23 Å, the Cr–S–Cr bond angle from 78° to 85°, and the interchain distance from 7.82 Å to 8.95 Å. Even with these structural perturbations, all chemical

bonding and symmetry around Cr and S is maintained. The ability to modulate these parameters, which should dictate both the direct and super-exchange coupling of the Cr centers while preserving the high symmetry of this system illustrates the power of reticular CP chemistry and provides an ideal opportunity to study 1D magnetic coupling schemes.

### *Magnetic Properties*

Variable-temperature magnetic susceptibility was measured on polycrystalline samples of **1** and **2** via SQUID magnetometry from 1.8 K to 300 K and presented as  $\chi T$  vs  $T$  in Figure 3. The effective magnetic moments  $\mu_{\text{eff}}$  of **1** and **2** are  $3.04 \mu_{\text{B}}$  and  $4.16 \mu_{\text{B}}$  per Cr respectively at 300 K. The theoretical spin-only value for  $S = 3/2$  Cr(III) centers is ( $3.87 \mu_{\text{B}}$ ), consistent with the measured moment of **2**, suggesting little contribution from spin-orbit coupling (SOC). A lack of SOC is consistent with the measured Cr XPS (Fig. S3). The lower value for **1** might suggest antiferromagnetic coupling, and indeed **1** and **2** show very different magnetic properties upon cooling, consistent with this hypothesis. While **1** shows a continuous decrease in susceptibility, the  $\chi T$  of **2** increases until a peak at 4.8 K. The temperature dependence of  $1/\chi$  above 100 K follows the Curie-Weiss law with a Curie constants  $C = 1.57$  and  $1.85 \text{ cm}^3 \text{ mol}^{-1}$  and Weiss constants  $\theta = -161$  and  $22.7$  K (Fig. S14 and Table S14.1). The Weiss constant sign suggests dominant AFM and FM coupling for **1** and **2** respectively.

Given the uniform chain structure of classical spin centers, we applied the Bonner-Fisher model based on the Hamiltonian  $H = -2J \sum (S_i \cdot S_{i+1})$ , given by Equation 1,<sup>16,50,51</sup> in order to estimate the intrachain magnetic coupling parameter  $J = J_{\text{NN}}$ .

$$\chi_m = \frac{N_A g^2 \mu_B^2 S(S+1)}{3k_B T} \left( \frac{1+u}{1-u} \right) \quad (1)$$

$$u = \coth\left(\frac{2JS(S+1)}{k_B T}\right) - \frac{k_B T}{2JS(S+1)}$$

Measured magnetic susceptibility curves with Bonner-Fisher fits for **1** and **2** are shown in Fig. 3 and provide coupling constants  $J_{\text{NN}}$  of  $-32.0(5)$  K and  $+5.7(1)$  K. The  $g$  values obtained from these fits are  $2.04(2)$  and  $1.98(1)$  respectively with  $S = 3/2$ , supporting no significant SOC contributions in these materials. The sign of the magnetic coupling switches between the two materials consistent with a switch from AFM to FM coupling and the observed experimental trends. Spin-polarized DFT calculations also support this switch between **1** and **2** (see below, Fig. S10).

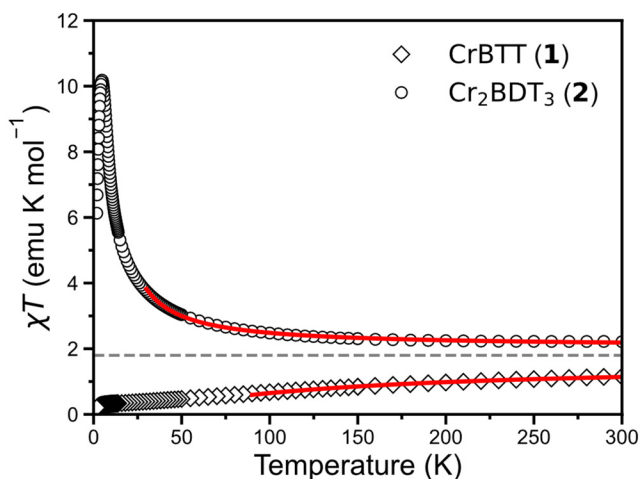


**Figure 3.** Experimental  $\chi T$  curves ( $\chi$  being magnetic susceptibility per mol Cr) measured from 1.8 K to 300 K under external magnetic field of 1000 Oe, with corresponding fit to the BF model given by equation 1 (red). CrBTT (**1**, black diamonds)  $J_{\text{NN}} = -32.0$  K, fit above  $T = 90$  K.  $\text{Cr}_2\text{BDT}_3$ , (**2**, black circles)  $J_{\text{NN}} = +5.7$  K, fit above  $T = 30$  K. (Grey dash)  $\chi T = 1.87$ , the high T spin-only limit for  $S = 3/2$ .

The observed change in the sign of  $J$  is noteworthy as all other examples of  $\text{Cr}_2(\text{SR})_3$  systems exhibit AFM exchange (Fig. S11).<sup>41,42,52,53</sup> The typical discussion of these systems invokes the Cr–Cr distance and dominant direct exchange between Cr centers. However, there should also be a significant superexchange interaction through the thiolate linkages. While any direct exchange between Cr centers should simply decrease as the Cr–Cr distance increases, the geometric dependence of the superexchange mechanism should be more complex, but can be interpreted through application of the Goodenough-Kanamori-Anderson (GKA) selection rules for magnetic coupling.<sup>54,55</sup> According to the GKA rules, in the general case of an octahedral,  $d^3$  center, where metal  $e_g$  orbital spins couple through a  $p_x$  ligand orbital, one expects superexchange to be AFM.<sup>54,56</sup> However, GKA predicts the electron superexchange contribution through a diamagnetic anion such as  $\text{RS}^-$  will become FM as the M–L–M angle approaches  $90^\circ$  due to the orthogonality of the contributing orbitals. Thus, the expectation is that the  $J$  coupling constant should become less negative as the angle approaches  $90^\circ$  along with a concomitant increase in the Cr–Cr distance.

We might expect strong superexchange interactions as bridging thiolates have been observed to facilitate greater superexchange coupling than  $\text{HO}^-$ ,  $\text{RN}^-$  and  $\text{Cl}^-$  as a result of enhanced covalency.<sup>52,57</sup> Quantifying the degree of direct vs super exchange, particularly in net AFM cases, is extremely challenging with limited examination by magneto-optical methods in the literature and much of the analysis focuses on the length of M–M distances for direct exchange as mentioned above.<sup>58–60</sup> In the present case quantifying the decrease in magnitude of the AFM direct exchange contribution from Cr–Cr when comparing **1** to **2** remains convoluted. However, the FM superexchange becomes demonstrably greater. As no other examples of FM coupling in  $\text{Cr}_2(\text{SR})_3$  motifs have been reported, and the Cr–S–Cr angle is nearly a perfect  $90^\circ$  ( $85^\circ$ ) in **2**, we propose that superexchange interactions, as predicted by the GKA rules, drive the observed switch in

magnetic interactions. The relatively smaller magnitude of the FM coupling can be rationalized by weaker overlap and is consistent with other literature examples and as is generally predicted by the theory behind the GKA rules.<sup>61–63</sup>

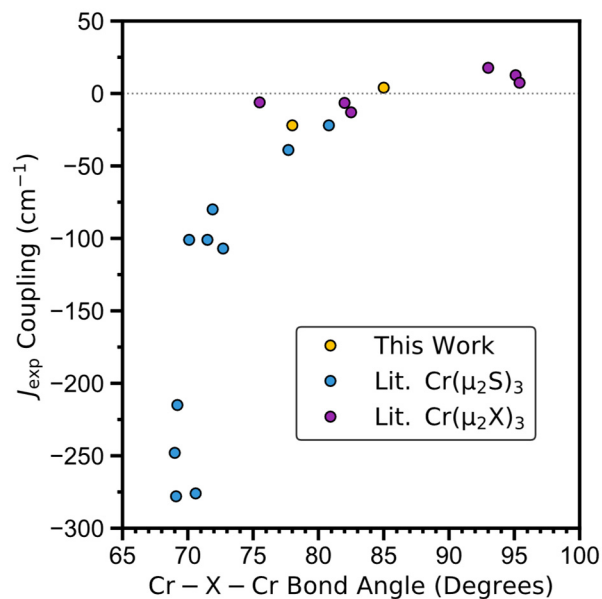


**Figure 4.** Experimental J-coupling values of tri-bridged Cr species in the literature covering both materials and molecular dimers. Given for all species found where magnetic and crystallographic data were reported. See S11 for detailed information and references.

This proposal is supported by the fact that previously reported Cr<sub>2</sub>(SR)<sub>3</sub> systems, which are all AFM, have Cr-S-Cr angles between 69 to 81° (Fig. 4). Indeed, complex **1** which is also AFM, similarly has a Cr-S-Cr angle of 78°. By contrast, the Cr-S-Cr angle of compound **2** is 85°, significantly closer to 90° than previous examples. This angle may be better contextualized versus the Cr trihalides, CrX<sub>3</sub>, which have Cr-X-Cr bond angles between 93 to 95° and all display FM behavior.<sup>64,65,61</sup> Similarly, angular deviation of ~8-10% has been estimated to limit the AFM/FM switch for 180° superexchange pathways in perovskites.<sup>66,67</sup> Finally, it is compelling to note that

the magnetic properties of **1** vs. **2** are primarily altered via structural or steric manipulation and not by changes to the ligand field or electronic differences between BDT and BTT. We hypothesize that this dramatic change in magnetic behavior, which can be thought of as arising from a compression along the chain-axis, could result in novel piezomagnetic or magnetostrictive properties under high pressure similar to what has been observed in layered  $\text{CrCl}_3$  and  $\text{CrI}_3$ .<sup>65,68,69</sup>

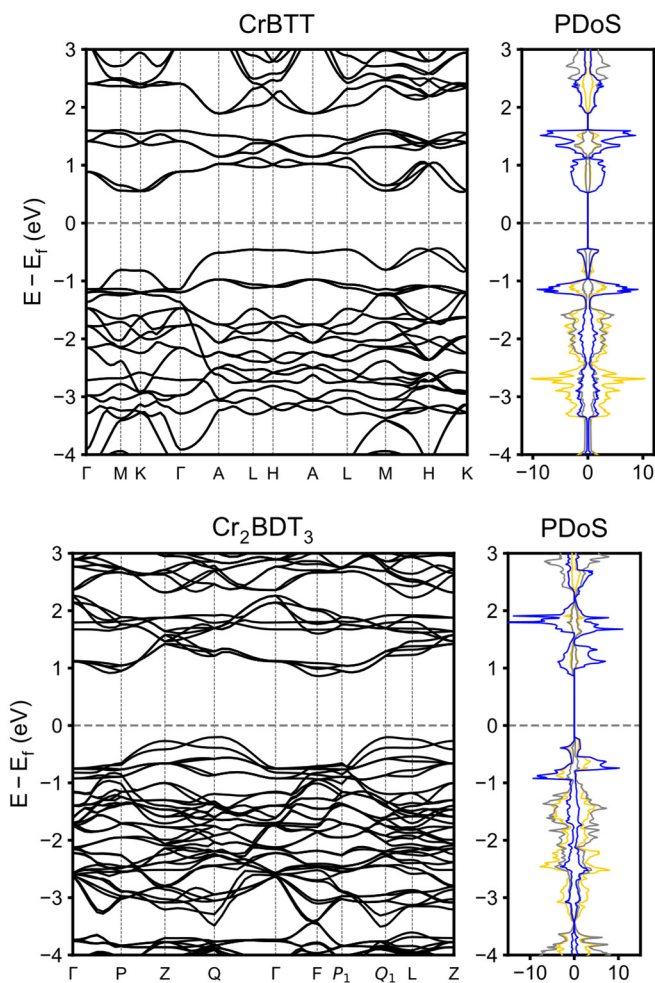


**Figure 5.** The band diagrams for CrBTT (**1**, top) and  $\text{Cr}_2\text{BDT}_3$  (**2**, bottom) near the Fermi level with the corresponding, spin-polarized projected partial density of states (PDoS); Blue = Cr 3d, yellow = S 2p, grey = C 2p. Calculated direct bandgap of **1** = 1.49 eV, **2** = 1.58 eV.

### *Electronic Structure and DFT Calculations*

The electronic structure of the crystalline structures of both **1** and **2** was examined with Density Functional Theory (DFT) calculations (Fig. 5). Calculations were performed across multiple functionals including GGA and hybrid, which all provide similar results within 1 meV per atom. For simplicity, we discuss the PBEsol values. The electronic structures near the bandgap are qualitatively comparable to the expected 2-1-2 crystal field splitting of a  $D_{3d}$  metal ion. The conduction band and first subvalence band are comprised of Cr  $e_g$  and Cr  $e_g'$  orbitals respectively, both with heavy mixing of S  $p_{xy}$  character indicative of strong Cr–S covalency (Fig. S12). The valence band itself is derived from the  $a_{1g}$  set in both **1** and **2**, arising from bonding Cr  $dz^2 + S p$  interactions. No direct Cr-Cr bonding interactions are observed in either species, implying there is no formal metal-metal bond.

UV-vis spectra of **1** and **2** were acquired via diffuse reflectance spectroscopy in order to experimentally measure the optical electronic properties of these systems. Both materials show broad absorptions above 2.0 eV with visible shoulders at slightly lower energy near 1.6 eV (Fig. 6). Tauc plot analysis of these shoulders reveals estimated optical bandgaps of 1.57 and 1.64 eV for **1** and **2** respectively (Fig. S13), which are within 0.1 eV of the calculated direct bandgaps by DFT (1.49 and 1.58 eV). These relatively weak shoulder transitions are consistent with the very small density of states (DoS) predicted near the valence band edge in both materials. Considering both the computed band structure along with the UV-Vis spectra, we assign (by analogy to d-d transitions) the shoulder as arising from a pseudo- $a_{1g}$  to  $e_g$  transition and the stronger onset above 2 eV as arising from pseudo- $e_g'$  to  $e_g$  transitions in both materials.

We do note that the calculated band structures reveal indirect band gaps approximately 0.4 eV smaller than the observed transitions, however Tauc analysis and DFT comparison both support

the observed transitions as being direct. Convolution from scattering or the Urbach tails of any direct transitions makes measurement of potential indirect transitions in this region unlikely. The predicted larger direct bandgap is also in line with the low measured bulk conductivity of the samples  $\sigma = 9.8 \times 10^{-4}$  S/m and  $5.2 \times 10^{-4}$  S/m for **1** and **2** respectively (Fig. S14). The band structures themselves have notable flatness in both the valence and conduction bands along the k-path A–L–H in **1** (hexagonal cell) and  $\Gamma$ –F–P<sub>1</sub> in **2** (rhombohedral cell). The lack of dispersion along these points implies that electron conductivity will be dependent on the crystallographic direction; considering the k-point symmetry, the conductivity should be greater along the axial direction of the Cr–S chains in these cases. The powder nature of these samples, however, prevents us from investigating anisotropic conductivity.

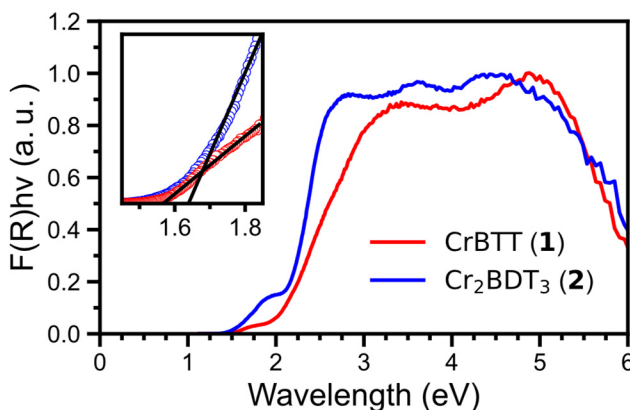


**Figure 6.** Normalized diffuse reflectance spectra for CrBTT (**1**, red) and Cr<sub>2</sub>BDT<sub>3</sub> (**2**, blue) (Inset) Corresponding Tauc plot near the band edge with extrapolation of the linear region as black lines. Experimental bandgaps via Tauc fitting: **1** = 1.57 eV, **2** = 1.64 eV (Fig S12).

As mentioned above, DFT was also used to estimate the  $J$  coupling values of the materials. This was done using the Heisenberg-Dirac-van-Vleck Hamiltonian in conjunction with the broken symmetry method.<sup>70</sup> The resulting estimated values of  $J_{NN}$  were  $-38$  K and  $33$  K for **1** and **2** respectively. While qualitatively correct, these values overestimate the magnitude of the



experimentally determined data, especially in the case of **2**. DFT is well-known to overestimate  $J$  coupling values owing to systematic over-localization of electrons in the DFT method.<sup>70–72</sup> Despite the overestimation of the magnitude of the coupling constants, all DFT calculations across multiple functionals and methods reproduce the key switch in the sign of  $J$  from experiment. We also used DFT with magnetic supercells to calculate the interchain coupling,  $J_1$  (Fig. S10). Converging many-atom systems with small energy differences, as required here, is exponentially more difficult than the primitive cells, however we were able to estimate interchain constants that are approximately 20-40 times smaller than the primary coupling constant (Fig S10). This result supports that omitting  $J_1$  in fitting experimental data to the Bonner-Fisher model via eq. 1 is a valid assumption and that the Cr(SR)<sub>3</sub> chains are appropriately considered 1D in their magnetic properties.

## Conclusion

We have demonstrated the synthesis of a novel pair of Cr thiolate CP structures using air-free solvothermal techniques. The compounds CrBTT and Cr<sub>2</sub>BDT<sub>3</sub> are novel pseudo-1D structures as determined by PXRD and Rietveld refinement in conjunction with EXAFS. The stacked octahedra motif is analogous to some structures such as the hexagonal perovskites. However, the unbroken repetition of the face connectivity and lack of alternating trigonal prismatic or rutile metal centers is quite rare in the literature and offers a more symmetric, tractable geometry for magnetic analysis than many pseudo 1D materials to date.

Magnetic susceptibility data for **1** and **2** were collected from 1.8 K to 300 K. Despite the identical structural bonding, the two materials were measured to have entirely different magnetic behavior with Cr ions in **1** being AFM coupled and **2** being FM coupled. Temperature dependent

magnetic susceptibilities were fit to the Bonner-Fisher model of 1D magnetism yielding intrachain coupling constants  $J_{NN}$  of  $-32.0(5)$  K and  $+5.7(1)$  K for **1** and **2** respectively. We explain this magnetic behavior as a result of the angular constraints of superexchange as described by GKA theory. DFT calculations were performed in order to corroborate the magnetic properties as well as the band structure of the materials. Calculated bandgaps of 1.49 and 1.58 eV were found to agree with the measured optical bandgap by UV-Vis reflectance data to within 0.1 eV.

Low dimensional magnetic materials represent an exciting class of systems for many applications. Maic 1 and 2D CPs which couple long-range crystalline order with magnetic and electronic properties are well-poised in this area. The ability to switch between FM and AFM regimes purely by synthetic, reticular tuning of the *c* lattice parameter and theoretically via external pressure represent potentially powerful methods for controlling material magnetic properties such as magnetoresistivity and magnetostriction.

## Experimental Section

Unless otherwise stated all manipulations were carried out in an airfree nitrogen glovebox or on a nitrogen Schlenk line using standard airfree Schlenk techniques and glassware. Solvents including DMF, acetonitrile, and ether were dried using a solvent purification still under Argon, filtered over alumina, and stored over 4 Å molecular sieves until used. Anhydrous  $\text{CrCl}_2$  was purchased from Alfa Aesar and used without further purification. Chromium metal (50 mesh) was purchased from Sigma-Aldrich. ICP standards were purchased from High Purity Standards. Trace metal grade nitric acid and hydrogen peroxide were purchased from Sigma-Aldrich. 1,4-dibromobenzene, 1,3,5-tribromobenzene, and 2-propanethiol were purchased from Sigma-Aldrich.

### *Preparation of Cr(OTf)<sub>2</sub>·2MeCN*

Salts of Cr(OTf)<sub>2</sub> were prepared by an adapted literature method.<sup>73</sup> A round bottom flask was connected to a nitrogen Schlenk line and was charged with 50 mL of deionized H<sub>2</sub>O then deoxygenated under dynamic vacuum for 2 hr. Cr metal powder (6 g, 115 mmol, 50 mesh) was added to flask followed by 10 mL of 40% triflic acid. The flask was brought to 50 °C in an oil bath and stirred for 4 hr over which time a vibrant blue developed. After cooling, an airfree frit with ground joints was inserted and the solution was filtered directly into a second Schlenk flask under N<sub>2</sub> to remove unreacted Cr metal. Excess water was removed under reduced pressure at 65 °C and the remaining solid was brought into the glovebox. The hydrated Cr salt does work towards the syntheses of **1** and **2**. Removing the hydrate was performed by three repeated recrystallizations from concentrated DMF or MeCN using layered Et<sub>2</sub>O as a counter solvent. Large millimeter size crystals are obtainable from this route and the resulting powders are pale blue after being dried under dynamic vacuum.

### *Preparation of the Ligands BDT and BTT*

Ligand 1,4-benzene dithiol (BDT) was prepared as described previously<sup>29</sup> and 1,3,5-benzene trithiol (BTT) was prepared using a similar but modified procedure.

### *1,3,5-tris(isopropylthio)benzene*

A 500 mL round bottom flask was charged with nitrogen on the Schlenk line. Powdered NaH (60% in mineral oil) was added to the flask (8.6 g, 215 mmol) and was washed twice with petroleum ether with decanting. The flask was then charged with 150 mL of DMF dried over

molecular sieves and degassed under vacuum for 1 hr. Using a dropping funnel, 20 mL (215 mmol) of 2-propane thiol was added slowly over 1 hr taking care to avoid excessive foaming, resulting in an opaque yellow mixture. Next 11.3 g (36 mmol) of 1,3,5-tribromobenzene was added to the flask and the oil bath was heated to 100 °C for 14 hr, resulting in a clear orange solution with white precipitate. After cooling the solution was diluted with 100 mL water and extracted three times with 50 mL of diethyl ether, followed by 5 washes with 50 mL of water. The organic layer was concentrated and filtered through a silica plug using 50/50 benzene/hexanes and dried yielding pure bright orange 1,3,5-tris(isopropylthio)benzene as an oil. Yield 9.0 g, 80%. The obtained product is spectroscopically identical to previous literature reports. <sup>1</sup>H NMR (400 MHz, benzene-d<sub>6</sub>) δ 6.86 (t, J = 1.3 Hz, 3H), 2.77 (hept, J = 6.7 Hz, 3H), 0.79 (d, J = 6.7 Hz, 18H).

#### *1,3,5-benzenetrithiol*

A 500 mL round-bottomed flask equipped to the Schlenk line was charged with 100 mL of dried DMA followed by 6.0 g (20 mmol) of 1,3,5-tris(isopropylthio)benzene and 2.3 g (100 mmol) Na metal. The flask was heated to 100 °C for 3 hr, bubbling vigorously and developing thick yellow precipitate. Once the bubbling subsided the flask was cooled before adding a second portion of 2.3 g (100 mmol) Na metal and heating to 100 °C again for 3 hr. The flask was then cooled in an ice bath and 60 mL of 10% HCl solution was slowly added via syringe dissolving most of the precipitate. Next the mixture was extracted three times with 50 mL of diethyl ether, followed by 5 washes with 50 mL of water. Upon drying the crude benzene trithiol was recrystallized from layered DCM and hexanes yielding pale yellow flakes. The obtained product is spectroscopically identical to previous literature reports.<sup>73</sup> <sup>1</sup>H NMR (400 MHz, benzene-d<sub>6</sub>) δ 6.45 (s, 3H), 2.80 (s, 3H).

### *Synthesis of CrBTT (1)*

In a glovebox 19 mg (0.15 mmol, 1.0 eq) of CrCl<sub>2</sub> and 33 mg (0.19 mmol, 1.25 eq) of BTT are dissolved in 4 mL DMF in a thick-walled glass vial and capped. The vessel is placed in a heating block and maintained at 120 °C for 16 hr. Over the course of the reaction red-brown precipitate is formed. After cooling the precipitate is removed from the vessel and separated by centrifugation. The material is purified by repeated suspension and centrifugation three times each in ~1 mL of DMF, MeCN, and Et<sub>2</sub>O. The final product is dried under vacuum yielding free flowing dark red powder. Yield 15 mg, 69%.

### *Synthesis of Cr<sub>2</sub>BDT<sub>3</sub> (2)*

Substituting BDT alone for the above procedure does not yield **2**. In a glovebox 43 mg (0.1 mmol) of Cr(OTf)<sub>2</sub>·2MeCN and 29 mg (0.2 mmol) of BDT are dissolved in 4 mL of acetonitrile. A solution of 35 μL (0.5 mmol, 5 eq) pyridine in 1 mL acetonitrile is prepared and added dropwise with stirring to the Cr solution at room temperature. The reaction is allowed to stir for 6 hr at room temperature yielding a red-brown precipitate which is isolated identically to CrBTT. Identical washing is performed as to **1** yielding a dark red powder. Yield 21 mg, 81%.

### **Conflicts of interest**

There are no conflicts to declare.

### **Preprints**

Ritchhart, A.; Filatov, A. S.; Jeon, I.-R.; Anderson, J. S. The Structure and Magnetic Properties of a New Family of 1D Chromium Thiolate Coordination Polymers, *ChemRxiv*, **2022**, <https://doi.org/10.26434/chemrxiv-2022-stt9q>

### **Supporting Information**

Additional experimental information and computational details. Including TGA, XPS, IR, EXAFS, SQUID, BET, NMR data and supporting references (PDF). Crystallographic data for **1** and **2** (CIF).

### **Acknowledgements**

This research was supported by the U.S. National Science Foundation (DMR-2002367), by a FACCTS grant through the France Chicago Center JSA gratefully acknowledges support from a Dreyfus Teacher-Scholar award (TC-21-064). This work made use of the shared facilities at the University of Chicago Materials Research Science and Engineering Center, supported by the National Science Foundation under award number DMR-2011854. MRCAT operations are supported by the Department of Energy and the MRCAT member institutions. This research used resources of the Advanced Photon Source beamline 10-BM, a Department of Energy (DOE) Office of Science User Facility operated for the DOE Office of Science by Argonne National Laboratory under Contract No. DE-AC02-06CH11357. Dr. Jorge Martinez and Dr. Pat Crossland are thanked for their assistance with XAS measurements.

### **References**

- (1) Bray, J. W.; Hart, H. R.; Interrante, L. V.; Jacobs, I. S.; Kasper, J. S.; Watkins, G. D.; Wee, S. H.; Bonner, J. C. Observation of a Spin-Peierls Transition in a Heisenberg Antiferromagnetic Linear-Chain System. *Phys. Rev. Lett.* **1975**, *35* (11), 744–747.
- (2) Kim, W.; Nair, S. Membranes from Nanoporous 1D and 2D Materials: A Review of Opportunities, Developments, and Challenges. *Chem. Eng. Sci.* **2013**, *104*, 908–924.
- (3) Bernardi, M.; Ataca, C.; Palummo, M.; Grossman, J. C. Optical and Electronic Properties of Two-Dimensional Layered Materials. *Nanophotonics* **2017**, *6* (2), 479–493.
- (4) Fan, S.; Feng, X.; Han, Y.; Fan, Z.; Lu, Y. Nanomechanics of Low-Dimensional Materials for Functional Applications. *Nanoscale Horiz.* **2019**, *4* (4), 781–788.
- (5) Kaner, R. B.; Allen, M. J.; Tung, V. C., Honeycomb Carbon: A Review of Graphene. *Chem. Rev.* **2010**, *110*, 1, 132–145
- (6) Ye, S.; Rathmell, A. R.; Chen, Z.; Stewart, I. E.; Wiley, B. J. Metal Nanowire Networks: The Next Generation of Transparent Conductors. *Adv. Mater.* **2014**, *26* (39), 6670–6687.
- (7) Hor, Y. S.; Xiao, Z. L.; Welp, U.; Ito, Y.; Mitchell, J. F.; Cook, R. E.; Kwok, W. K.; Crabtree, G. W. Nanowires and Nanoribbons of Charge-Density-Wave Conductor NbSe<sub>3</sub>. *Nano Lett.* **2005**, *5* (2), 397–401.
- (8) Esmaeil Zadeh, I.; Chang, J.; Los, J. W. N.; Gyger, S.; Elshaari, A. W.; Steinhauer, S.; Dorenbos, S. N.; Zwiller, V. Superconducting Nanowire Single-Photon Detectors: A Perspective on Evolution, State-of-the-Art, Future Developments, and Applications. *Appl. Phys. Lett.* **2021**, *118* (19), 190502.
- (9) Gibertini, M.; Koperski, M.; Morpurgo, A. F.; Novoselov, K. S. Magnetic 2D Materials and Heterostructures. *Nat. Nanotechnol.* **2019**, *14* (5), 408–419.
- (10) Jiang, X.; Liu, Q.; Xing, J.; Liu, N.; Guo, Y.; Liu, Z.; Zhao, J. Recent Progress on 2D Magnets: Fundamental Mechanism, Structural Design and Modification. *Appl. Phys. Rev.* **2021**, *8* (3), 031305.
- (11) Fert, A.; Cros, V.; Sampaio, J. Skyrmions on the Track. *Nat. Nanotechnol.* **2013**, *8* (3), 152–156.
- (12) Tejada, J.; Chudnovsky, E. M.; Barco, E. del; Hernandez, J. M.; Spiller, T. P. Magnetic Qubits as Hardware for Quantum Computers. *J. Nanotechnol.* **2001**, *12* (2), 181–186.
- (13) Terada, N.; Mamiya, H. High-Efficiency Magnetic Refrigeration Using Holmium. *Nat. Commun.* **2021**, *12* (1), 1212.
- (14) Vieira, N. C.; Avansi, W.; Figueiredo, A.; Ribeiro, C.; Mastelaro, V. R.; Guimarães, F. E. Ion-Sensing Properties of 1D Vanadium Pentoxide Nanostructures. *Nanoscale Res. Lett.* **2012**, *7* (1), 310.
- (15) Jose, R.; Kancharlapalli, S.; Ghanty, T. K.; Pal, S.; Rajaraman, G. The Decisive Role of Spin States and Spin Coupling in Dictating Selective O<sub>2</sub> Adsorption in Chromium(II) Metal–Organic Frameworks. *Chem. Eur. J.* **2022**, *28* (18), e202104526.
- (16) Brush, S. G. History of the Lenz-Ising Model. *Rev. Mod. Phys.* **1967**, *39* (4), 883–893.
- (17) Jana, S.; Aich, P.; Kumar, P. A.; Forslund, O. K.; Nocerino, E.; Pomjakushin, V.; Månsson, M.; Sassa, Y.; Svedlindh, P.; Karis, O.; Siruguri, V.; Ray, S. Revisiting Goodenough-Kanamori Rules in a New Series of Double Perovskites LaSr<sub>1-x</sub>Ca<sub>x</sub>NiReO<sub>6</sub>. *Sci. Rep.* **2019**, *9* (1), 18296.
- (18) Valldor, M.; Morrow, R. Bichalcogenide Model Systems for Magnetic Chains with Variable Spin Sizes and Optional Crystallographic Inversion Symmetry. *Inorg. Chem.* **2019**, *58* (18), 11978–11982.

- (19) Saha-Dasgupta, T. The Fascinating World of Low-Dimensional Quantum Spin Systems: Ab Initio Modeling. *Molecules* **2021**, *26* (6), 1522.
- (20) López-Cabrelles, J.; Mañas-Valero, S.; Vitorica-Yrezabal, I. J.; Bereciartua, P. J.; Rodríguez-Velamazán, J. A.; Waerenborgh, J. C.; Vieira, B. J. C.; Davidovikj, D.; Steeneken, P. G.; van der Zant, H. S. J.; Mínguez Espallargas, G.; Coronado, E. Isorecticular Two-Dimensional Magnetic Coordination Polymers Prepared through Pre-Synthetic Ligand Functionalization. *Nat. Chem.* **2018**, *10* (10), 1001–1007.
- (21) Gruzdev, M.; Chervonova, U.; Kolker, A.; Fomina, N.; Zueva, E.; Vorobeva, V.; Starichenko, D.; Korolev, A. Dendritic Iron(III) Carbazole Complexes: Structural, Optical, and Magnetic Characteristics. *Materials* **2021**, *14* (18), 5445.
- (22) Coulon, C.; Miyasaka, H.; Clérac, R. Single-Chain Magnets: Theoretical Approach and Experimental Systems. In *Single-Molecule Magnets and Related Phenomena*; Winpenny, R., Ed.; Structure and Bonding; Springer: Berlin, Heidelberg, 2006; pp 163–206.
- (23) Miyasaka, H.; Julve, M.; Yamashita, M.; Clérac, R. Slow Dynamics of the Magnetization in One-Dimensional Coordination Polymers: Single-Chain Magnets. *Inorg. Chem.* **2009**, *48* (8), 3420–3437.
- (24) Jeon, I.-R.; Clérac, R. Controlled Association of Single-Molecule Magnets (SMMs) into Coordination Networks: Towards a New Generation of Magnetic Materials. *Dalton Trans.* **2012**, *41* (32), 9569–9586.
- (25) Maignan, A.; Michel, C.; Masset, A. C.; Martin, C.; Raveau, B. Single Crystal Study of the One Dimensional CaCoO Compound: Five Stable Configurations for the Ising Triangular Lattice. *Eur. Phys. J. B* **2000**, *15* (4), 657–663.
- (26) Qu, Y.; Arguilla, M. Q.; Zhang, Q.; He, X.; Dincă, M. Ultrathin, High-Aspect Ratio, and Free-Standing Magnetic Nanowires by Exfoliation of Ferromagnetic Quasi-One-Dimensional van Der Waals Lattices. *J. Am. Chem. Soc.* **2021**, *143* (46), 19551–19558.
- (27) Vrbani, D.; Remkar, M.; Jesih, A.; Mrzel, A.; Umek, P.; Ponikvar, M.; Janar, B.; tjan; Meden, A.; Novosel, B.; Pejovnik, S.; Venturini, P.; Coleman, J. C.; Mihailovi, D. Air-Stable Monodispersed Mo<sub>6</sub>S<sub>3</sub>I<sub>6</sub> Nanowires. *J. Nanotechnol.* **2004**, *15* (5), 635–638.
- (28) Ji, Z.; Trickett, C.; Pei, X.; Yaghi, O. M. Linking Molybdenum–Sulfur Clusters for Electrocatalytic Hydrogen Evolution. *J. Am. Chem. Soc.* **2018**, *140* (42), 13618–13622.
- (29) Horwitz, N. E.; Xie, J.; Filatov, A. S.; Papoular, R. J.; Shepard, W. E.; Zee, D. Z.; Grahn, M. P.; Gilder, C.; Anderson, J. S. Redox-Active 1D Coordination Polymers of Iron–Sulfur Clusters. *J. Am. Chem. Soc.* **2019**, *141* (9), 3940–3951.
- (30) Liang, T.; Koohpayeh, S. M.; Krizan, J. W.; McQueen, T. M.; Cava, R. J.; Ong, N. P. Heat Capacity Peak at the Quantum Critical Point of the Transverse Ising Magnet CoNb<sub>2</sub>O<sub>6</sub>. *Nat. Commun.* **2015**, *6* (1), 7611.
- (31) Dietzel, P. D. C.; Morita, Y.; Blom, R.; Fjellvåg, H. An In Situ High-Temperature Single-Crystal Investigation of a Dehydrated Metal–Organic Framework Compound and Field-Induced Magnetization of One-Dimensional Metal–Oxygen Chains. *Angew. Chem. Int. Ed.* **2005**, *44* (39), 6354–6358.
- (32) Lescouëzec, R.; Vaissermann, J.; Ruiz-Pérez, C.; Lloret, F.; Carrasco, R.; Julve, M.; Verdaguer, M.; Dromzee, Y.; Gatteschi, D.; Wernsdorfer, W. Cyanide-Bridged Iron(III)–Cobalt(II) Double Zigzag Ferromagnetic Chains: Two New Molecular Magnetic Nanowires. *Angew. Chem. Int. Ed.* **2003**, *42* (13), 1483–1486.

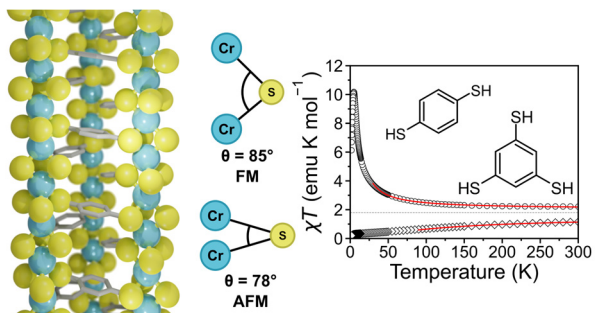


- (33) Abakumov, A. M.; Shpanchenko, R. V.; Antipov, E. V.; Lebedev, O. I.; Tendeloo, G. V.; Amelinckx, S. Synthesis and Structural Study of Hexagonal Perovskites in the  $\text{Ba}_5\text{Ta}_4\text{O}_{15}\text{-MZrO}_3$  (M=Ba, Sr) System. *J. Solid State Chem.* **1998**, *141* (2), 492–499.
- (34) de Jongh, L. J.; Miedema, A. R. Experiments on Simple Magnetic Model Systems. *Adv. Phys.* **1974**, *23* (1), 1–260.
- (35) Castner, D. G.; Hinds, K.; Grainger, D. W. X-Ray Photoelectron Spectroscopy Sulfur 2p Study of Organic Thiol and Disulfide Binding Interactions with Gold Surfaces. *Langmuir* **1996**, *12* (21), 5083–5086.
- (36) Bourg, M.-C.; Badia, A.; Lennox, R. B. Gold–Sulfur Bonding in 2D and 3D Self-Assembled Monolayers: XPS Characterization. *J. Phys. Chem. B* **2000**, *104* (28), 6562–6567.
- (37) Chu, H.; Noh, H.; Kim, Y.-J.; Yuk, S.; Lee, J.-H.; Lee, J.; Kwack, H.; Kim, Y.; Yang, D.-K.; Kim, H.-T. Achieving Three-Dimensional Lithium Sulfide Growth in Lithium-Sulfur Batteries Using High-Donor-Number Anions. *Nat. Commun.* **2019**, *10* (1), 188.
- (38) Toby, B. H.; Von Dreele, R. B. GSAS-II: The Genesis of a Modern Open-Source All Purpose Crystallography Software Package. *J. Appl. Cryst.* **2013**, *46* (2), 544–549.
- (39) Cordero, B.; Gómez, V.; Platero-Prats, A. E.; Revés, M.; Echeverría, J.; Cremades, E.; Barragán, F.; Alvarez, S. Covalent Radii Revisited. *Dalton Trans.* **2008**, *21*, 2832–2838.
- (40) Reardon, D.; Kovacs, I.; Rupp, K. B. P.; Feghali, K.; Gambarotta, S.; Petersen, J. Reactivity of Coordinatively Unsaturated Trivalent Chromium Complexes with Sulfur: Preparation of Novel Sulfide-Bridged Dinuclear Cr(IV) Derivatives. *Eur. J. Chem.* **1997**, *3* (9), 1482–1488.
- (41) Pasynskii, A. A.; Denisov, F. S.; Torubaev, Yu. V.; Semenova, N. I.; Novotortsev, V. M.; Ellert, O. G.; Nefedov, S. E.; Lyssenko, K. A. Antiferromagnetic Complexes with Metal-metal Bonds: Part XXIX. Synthesis and Molecular Structures of Heterochalcogenide Binuclear Complex  $[\pi\text{-(CH}_3\text{C}_5\text{H}_4\text{)Cr}(\mu\text{-SPh})]_2\text{Se}$  and Trinuclear Mixed-Metal Cluster  $[\pi\text{-(CH}_3\text{C}_5\text{H}_4\text{)}_2\text{Cr}_2(\mu\text{-SPh})(\text{M}_3\text{-S})(\text{M}_3\text{-Se})\text{Co}(\text{CO})_2]$ . *J. Organomet. Chem.* **2000**, *612* (1), 9–13.
- (42) Wei, N.; Yang, D.; Zhang, Y.; Wang, B.; Qu, J. Synthesis, Structure, and Oxidative Reactivity of a Class of Thiolate-Bridged Dichromium Complexes Featuring Antiferromagnetic Coupling Interactions. *Eur. J. Inorg. Chem.* **2021**, *2021* (10), 923–928.
- (43) Maignan, A.; Michel, C.; Masset, A. C.; Martin, C.; Raveau, B. Single Crystal Study of the One Dimensional  $\text{Ca}_3\text{Co}_2\text{O}_6$  Compound: Five Stable Configurations for the Ising Triangular Lattice. *Eur. Phys. J. B* **2000**, *15* (4), 657–663.
- (44) Fukuoka, H.; Miyaki, Y.; Yamanaka, S. High-Pressure Synthesis and Structures of Novel Chromium Sulfides,  $\text{Ba}_3\text{CrS}_5$  and  $\text{Ba}_3\text{Cr}_2\text{S}_6$  with One-Dimensional Chain Structures. *J. Solid State Chem.* **2003**, *176* (1), 206–212.
- (45) Fop, S.; McCombie, K. S.; Wildman, E. J.; Skakle, J. M. S.; Mclaughlin, A. C. Hexagonal Perovskite Derivatives: A New Direction in the Design of Oxide Ion Conducting Materials. *Chem. Commun.* **2019**, *55* (15), 2127–2137.
- (46) Wu, X.; Tao, Y.; Hu, Y.; Song, Y.; Hu, Z.; Zhu, J.; Dong, L. Tantalum Disulfide Nanobelts: Preparation, Superconductivity and Field Emission. *J. Nanotechnol.* **2005**, *17* (1), 201–205.
- (47) Pham, T.; Oh, S.; Stetz, P.; Onishi, S.; Kisielowski, C.; Cohen, M. L.; Zettl, A. Torsional Instability in the Single-Chain Limit of a Transition Metal Trichalcogenide. *Science* **2018**, *361* (6399), 263–266.
- (48) Yang, J.; Wang, Y. Q.; Zhang, R. R.; Ma, L.; Liu, W.; Qu, Z.; Zhang, L.; Zhang, S. L.; Tong, W.; Pi, L.; Zhu, W. K.; Zhang, C. J. Observation of Charge Density Wave Transition in  $\text{TaSe}_3$  Mesowires. *Appl. Phys. Lett.* **2019**, *115* (3), 033102.

- (49) Meyer, S.; Pham, T.; Oh, S.; Ercius, P.; Kisielowski, C.; Cohen, M. L.; Zettl, A. Metal-Insulator Transition in Quasi-One-Dimensional  $\text{HfTe}_3$  in the Few-Chain Limit. *Phys. Rev. B* **2019**, *100* (4), 041403.
- (50) Fisher, M. E. Magnetism in One-Dimensional Systems—The Heisenberg Model for Infinite Spin. *Am. J. Phys.* **1964**, *32* (5), 343–346.
- (51) Bonner, J. C.; Fisher, M. E. Linear Magnetic Chains with Anisotropic Coupling. *Phys. Rev.* **1964**, *135* (3A), A640–A658.
- (52) Schenker, R.; Weihe, H.; Güdel, H. U.; Kersting, B. Exchange Pathways in Tris- $\mu$ -Thiolato-Bridged  $[\text{Cr}_2\text{L}_3](\text{ClO}_4)_2\text{Cl}\cdot\text{H}_2\text{O}\cdot\text{MeOH}$  (L = 2,6-Bis(Aminomethyl)-4-Tert-Butyl-Thiophenolate). *Inorg. Chem.* **2001**, *40* (14), 3355–3362.
- (53) Goh, L. Y.; Tay, M. S.; Mak, T. C. W.; Wang, R. J. Thiolate-Bridged Dichromium Complexes. Syntheses and Crystal Structures of  $[\text{CpCr}(\text{CO})_2(\text{SPh})]_2$  and  $[\text{CpCr}(\text{SPh})]_2\text{S}$ . *Organometallics* **1992**, *11* (4), 1711–1717.
- (54) Goodenough, J. B. Theory of the Role of Covalence in the Perovskite-Type Manganites  $[\text{La}, \text{M}(\text{II})]\text{MnO}_3$ . *Phys. Rev.* **1955**, *100* (2), 564–573.
- (55) Kanamori, J. Theory of the Magnetic Properties of Ferrous and Cobaltous Oxides, I. *Prog. Theor. Phys.* **1957**, *17*, 177–196.
- (56) Anderson, P. W. New Approach to the Theory of Superexchange Interactions. *Phys. Rev.* **1959**, *115* (1), 2–13.
- (57) Monillas, W. H.; Yap, G. P. A.; Theopold, K. H. Reactivity of a Low-Valent Chromium Dinitrogen Complex. *Inorganica Chim. Acta* **2011**, *369* (1), 103–119.
- (58) Dubicki, L.; Ferguson, J.; Harrowfield, B. V. Exchange Interactions in a Trigonal Chromium(III) Pair: II.  ${}^4\text{A}_2$   ${}^2\text{E}$  Pair States in  $\text{Cs}_3\text{Cr}_2\text{Br}_9$ . *Mol. Phys.* **1977**, *34* (6), 1545–1561.
- (59) N. J. Dean; K. J. Maxwell. Exchange Studies in a Trigonal  $\text{Cr}^{3+}$  Dimer System: The ( ${}^4\text{A}_2 \times {}^2\text{E}$ ) and ( ${}^4\text{A}_2 \times {}^4\text{A}_2$ ) States in  $\text{Rb}_3\text{Cr}_2\text{Br}_9$ . *Chem. Phys.* **1986**, *106* (2), 233–242.
- (60) Morsing, T. J.; Bendix, J.; Weihe, H.; Døssing, A. Oxo-Bridged Dinuclear Chromium(III) Complexes: Correlation between the Optical and Magnetic Properties and the Basicity of the Oxo Bridge. *Inorg. Chem.* **2014**, *53* (6), 2996–3003.
- (61) Wang, M.-C.; Chang, C.-R. Goodenough-Kanamori-Anderson Rules in  $\text{CrI}_3/\text{MoTe}_2/\text{CrI}_3$  Van Der Waals Heterostructure. *J. Electrochem. Soc.* **2022**, *169* (5), 053507.
- (62) Zhang, F.; Kong, Y.-C.; Pang, R.; Hu, L.; Gong, P.-L.; Shi, X.-Q.; Tang, Z.-K. Super-Exchange Theory for Polyvalent Anion Magnets. *New J. Phys.* **2019**, *21* (5), 053033.
- (63) Koehler, W. C.; Wollan, E. O. Neutron-Diffraction Study of the Magnetic Properties of Perovskite-like Compounds  $\text{LaBO}_3$ . *J. Phys. Chem. Solids* **1957**, *2* (2), 100–106.
- (64) Tsubokawa, I. On the Magnetic Properties of a  $\text{CrBr}_3$  Single Crystal. *J. Phys. Soc. Jpn.* **1960**, *15* (9), 1664–1668.
- (65) Chen, S.; Huang, C.; Sun, H.; Ding, J.; Jena, P.; Kan, E. Boosting the Curie Temperature of Two-Dimensional Semiconducting  $\text{CrI}_3$  Monolayer through van Der Waals Heterostructures. *J. Phys. Chem. C* **2019**, *123* (29), 17987–17993.
- (66) Moskvina, A.; Ovanesyan, N.; Trukhtanov, V. Angular Dependence of the Superexchange Interaction  $\text{Fe}^{3+}\text{-O}_2\text{Cr}^{3+}$ . *Hyperfine Interact.* **1975**, *1*, 265–281.
- (67) Rao, C. N. R.; Arulraj, A.; Santosh, P. N.; Cheetham, A. K. Charge-Ordering in Manganates. *Chem. Mater.* **1998**, *10* (10), 2714–2722.

- (68) Ahmad, A. S.; Liang, Y.; Dong, M.; Zhou, X.; Fang, L.; Xia, Y.; Dai, J.; Yan, X.; Yu, X.; Dai, J.; Zhang, G.; Zhang, W.; Zhao, Y.; Wang, S. Pressure-Driven Switching of Magnetism in Layered CrCl<sub>3</sub>. *Nanoscale* **2020**, *12* (45), 22935–22944.
- (69) Bacaksiz, C.; Šabani, D.; Menezes, R. M.; Milošević, M. V. Distinctive Magnetic Properties of CrI<sub>3</sub> and CrBr<sub>3</sub> Monolayers Caused by Spin-Orbit Coupling. *Phys. Rev. B* **2021**, *103* (12), 125418.
- (70) Joshi, R. P.; Phillips, J. J.; Mitchell, K. J.; Christou, G.; Jackson, K. A.; Peralta, J. E. Accuracy of Density Functional Theory Methods for the Calculation of Magnetic Exchange Couplings in Binuclear Iron(III) Complexes. *Polyhedron* **2020**, *176*, 114194.
- (71) Weissman, S.; Antkowiak, M.; Brzostowski, B.; Kamieniarz, G.; Kronik, L. Accurate Magnetic Couplings in Chromium-Based Molecular Rings from Broken-Symmetry Calculations within Density Functional Theory. *J. Chem. Theory Comput.* **2019**, *15* (9), 4885–4895.
- (72) Pantazis, D. A. Meeting the Challenge of Magnetic Coupling in a Triply-Bridged Chromium Dimer: Complementary Broken-Symmetry Density Functional Theory and Multireference Density Matrix Renormalization Group Perspectives. *J. Chem. Theory Comput.* **2019**, *15* (2), 938–948.
- (73) Ocone, L. R.; Block, B. P.; Collman, J. P.; Buckingham, D. A. Anhydrous Chromium(II) Acetate, Chromium(II) Acetate 1-Hydrate, and Bis(2,4-Pentanedionato)Chromium(II). In *Inorganic Syntheses*; John Wiley & Sons, Ltd, 1966; Vol. 8, pp 125–132.

For Table of Contents Only



Sulfur-based coordination polymers are an emerging class of materials with relatively few known examples compared to oxygen-based compounds. Here we report the synthesis and magnetic properties of two new closely related Cr-thiolate coordination polymers. Both materials adopt a pseudo-1D structure with a coupled Cr chain motif. We examine the 1D magnetism that arises from this configuration and find it is highly dependent on the bond angle between Cr and S which dictates the magnetic coupling mechanism.